Journal of Machine Engineering, 2026, Vol. 26,
ISSN 1895-7595 (Print) ISSN 2391-8071 (Online) License CC-BY-NC 4.0

Received*: 28 May 2026* / Accepted: *20 November 2026* / Published online: *27 November 27 2026*

simulation,
additive manufacturing,
cold spray

Eckart UHLMANN[1,2], Thomas BRAUN[1*],
Xinyu ZHANG[1], Daniel PAVEL[1]

DEPOSITION MODELLING AND EXPERIMENTAL VALIDATION FOR COLD SPRAY ADDITIVE MANUFACTURING

Cold Gas Spraying, a thermal spray process originating in applications for wear and corrosion resistance coatings, is becoming increasingly relevant in the area of additive manufacturing (AM). Due to continuous advances in industrial robotics development, the cold spray process is considered a feasible process for the large-scale additive manufacturing of metallic components. However, compared to other robot-based AM-processes such as fused deposition modeling (FDM) or fused granular fabrication (FGF), cold spray additive manufacturing (CSAM) lacks sufficient simulation and prediction tools for the resulting material deposition geometry. This depends on both the spray parameters as well as the robotic parameters. A simulation tool has now been developed for pure copper and stainless steel 316L, providing a model to predict deposition geometries for manufacturing complex AM parts with CSAM. This paper describes the simulation model and its experimental validation on planar substrates. The results show a high simulation accuracy for single spray tracks, multi-track- and multi-layer-deposition, which provides a possibility for generic geometry generation. The results are the basis for a closed-loop, sensor-assisted control of the robot-based CSAM process.

1. INTRODUCTION

1.1. COLD SPRAY IN ADDITIVE MANUFACTURING

Cold spray is becoming increasingly important as an AM-process for the production of functional components. In particular, the technology offers considerable advantages for the fabrication of large-scale parts and complex geometries compared with conventional thermal spray processes. Among thermal spray-based manufacturing methods, cold spray is distinguished by its high deposition rate and its capability to build up substantial material volumes within short processing times. In this process, powder particles are heated and accelerated by a process gas, typically nitrogen or helium, through a Laval-nozzle. Upon impact with the substrate, particle velocities can reach up to approximately v_p = 1,000 m/s,

[1] Institute for Machine Tools and Factory Management (IWF), Technische Universität Berlin, Berlin, Germany
[2] Fraunhofer-Institute for Production Systems and Design Technology IPK, Berlin, Germany
[*] E-mail: braun@iwf.tu-berlin.de
https://doi.org/10.36897/jme/243120

resulting in plastic deformation and bonding without melting [1]. In layer-wise deposition, the final 3D-geometry is defined by the relative movement between the nozzle and the substrate. Due to its comparatively low process temperatures, cold spray minimizes thermally induced effects such as tensile residual stresses, which is a major advantage over many other thermal spray and additive manufacturing technologies [2–4].

These characteristics are especially relevant for the additive manufacturing of large technical components, where geometric distortion caused by residual stresses is a critical issue [5–7]. One example is the production of stiffening structures for railway car bodies. Traditionally, such structures are manufactured by welding. In contrast, cold spray additive manufacturing enables material to be deposited specifically in highly loaded regions, especially when combined with topology-optimized component designs. This creates significant potential for improving material efficiency while maintaining structural performance [8, 9].

At the same time, current research increasingly focuses on enhancing dimensional accuracy and surface quality in CSAM. A key objective is to reduce defects such as irregular deposition behavior and local surface imperfections in order to compensate deviations from the target geometry and enable near-net-shape manufacturing. This requires a deeper understanding of the underlying deposition mechanisms and the development of predictive approaches that account for both process conditions and component-specific requirements.

1.2. PROCESS AUTOMATION AND TOOL PATH PLANNING

For additive manufacturing of large and geometrically demanding structures, cold spray is frequently implemented as a robot-guided process. Mounting the spray gun on an industrial robot enables material deposition on curved and non-planar surfaces while also allowing deliberate adjustment of the spray angle γ. A prerequisite for such an approach is a reliable tool path planning strategy, since the generated path forms the basis for robot programming and therefore directly determines the nozzle movement during the process [10, 11]. The overarching aim is the reproducible production of near-net-shape components.

In this context, adaptive tool path planning is of particular importance, as it provides the foundation for controlling the material deposition systematically. One of the main challenges lies in maintaining a constant coating speed v_c, even during complex multi-axis robot movements. At the same time, the resulting deposition geometry depends strongly on the selected process parameters, the substrate geometry, and the deposition material. Consequently, tool path planning must not only define the nozzle trajectory but also account for process-related influences such as spray angle γ, coating speed v_c, and local geometric conditions.

The present work addresses this challenge by developing a simulation-supported approach to tool path planning for automated CSAM. The objective is to create a process-oriented basis for robot programming that minimizes deposition inconsistencies and surface defects through simulation and systematic control of material build-up. This provides a method for higher levels of process automation, including in situ monitoring and process adaptation by means of integrated sensor systems such as a laser profile sensor. Based on

measured deviations between the target and actual geometry, process parameters such as coating speed v_c and spray angle γ can subsequently be adjusted automatically to improve geometric accuracy.

1.3. SIMULATION APPROACH

In order to support an automated and adaptive manufacturing strategy, a predictive simulation of the deposition process is required. Although numerous studies have investigated particle impact behavior and deposition mechanisms in cold spray using mathematical, physical, and data-driven models, the transfer of these findings into comprehensive deposition simulations remains limited [12]. In many cases, existing models have been validated only for narrow parameter ranges and are therefore not directly suitable for multi-track deposition scenarios or for applications involving varying substrate geometries. In addition, many available simulation approaches were originally developed for other thermal spray processes and do not fully capture the specific physical principles of cold spray [13].

The present research therefore follows an effect-based and workpiece-centered modeling strategy that explicitly incorporates component-specific requirements into the simulation and subsequent path planning. The aim is to develop a multi-parameter simulation framework capable of predicting material deposition with high accuracy under realistic process conditions. This includes the consideration of key influencing variables such as coating speed v_c, spray angle γ, substrate geometry, and material system. By combining mathematical, physical, and data-based models, the simulation is intended to represent the deposition result in a way that is sufficiently accurate for process planning and future closed-loop control applications.

To validate this approach, experimental investigations are conducted using stainless steel 316L and pure copper as deposition materials. In addition to the overall deposition behavior, the influence of tool orientation and application strategy on both geometric properties and material integrity is examined. In this way, the simulation serves not only as a predictive tool for deposition behavior but also as a technological basis for automated tool path planning and the realization of near-net-shape CSAM.

2. EXPERIMENTAL SETUP

The cold spray system used to gain the experimental data is a spray gun 6/11 EvoCSII from IMPACT INNOVATIONS GMBH, Rattenkirchen, Germany. The experiments were performed with the two deposition materials, stainless steel 316L with a particle size of $15\ \mu m \leq d_{p,st} \leq 38\ \mu m$ from supplier SANDVIK OSPREY LIMITED, Neath, United Kingdom and pure copper with a particle size of $15\ \mu m \leq d_{p,cu} \leq 38\ \mu m$ from supplier SAFINA, A.S., Vestec, Czech Republic. Every experiment was repeated two times in a

randomized manner for statistical robustness. For the substrate material, aluminium type EN AW-6082 was used.

The cold spray parameters used for the deposition of stainless steel 316L were a gas temperature $T_{N_2,St}$ = 850°C and a gas pressure of $p_{N_2,St}$ = 5 MPa. For copper a gas temperature $T_{N_2,cu}$ = 750°C and a gas pressure of $p_{N_2,cu}$ = 5 MPa were used.

The steel 316L-material feed rate was uniformly set to $\dot{m}_{St}$ = 5.0 kg/h for all experiments. The copper material feed rate was set to $\dot{m}_{Cu}$ = 5.9 kg/h in the first experimental phase and $\dot{m}_{cu}$ = 4.2 kg/h in the subsequent phases due to high heat development in the specimen at multi-track and multi-layer experiments. The spray- and robotic parameters used in phase 1 are given in Table 1.

Table 1. Spray- and robotic parameters used in experimental phase 1 for deposition of pure copper and steel 316L

Process parameter	Unit	Parameter values			
Coating speed v_c	mm/s	250	375	500	
Nozzle distance a	mm	30	50	70	
Spray angle γ	°	0	15	30	45

Since the thickness of the coating plays a critical role in the process simulation, it is necessary to adjust the coating speed v_c for sufficient evaluation of the material deposition. Therefore, the coating speed v_c was set to parameters between 250 mm/s ≤ v_c ≤ 500 mm/s (Table 1). Also, the spray from the nozzle misaligns due to the diverging geometry of the spray plume, which could result in an uneven coating area influenced by the distance a between the nozzle and the substrate. In a first experimental phase, 108 planar substrate samples were coated for each material. These were used as a baseline to evaluate the particle distribution in straight single spray tracks in dependence on the nozzle distance a, the coating speed v_c and the spray angle γ. In the second phase, additional parameters were varied with respect to the application of several spray tracks in one coating layer. Here, the number of tracks applied in a zigzag-pattern n_t and the track distance in between the tracks d_t were varied, which resulted in 216 coated samples for each copper and steel 316L. The spray- and robotic parameters used in phase 2 are given in Table 2.

Table 2. Spray- and robotic parameters used in experimental phase 2 for deposition of pure copper and steel 316L

Process parameter	Unit	Parameter values			
Coating speed v_c	mm/s	250	375	500	
Nozzle distance a	mm	30		50	
Spray angle γ	°	0			
Number of tracks n_t	-	2	3	5	10
Track distance d_t	mm	0.5	1.0	1.5	

A third phase with 36 coated samples for each copper and steel 316L was carried out, in which the application of several layers was evaluated. Here, the number of applied layers n_l was varied. A subsequent phase will involve experiments with convex and concave substrate geometries to further refine the simulation model to account for the effects of varying substrate geometries. The spray- and robotic parameters used in phase 3 are given in Table 3.

To examine the material deposition from the experiment, a laser profile sensor type LJ-X8200 from KEYENCE DEUTSCHLAND GMBH, Frankfurt am Main, Germany was used for automated deposition measuring from surface increment scanning. Therefore, the laser sensor is mounted on the robot system above the cold spray gun to closely follow and scan the material deposition (Fig. 1).

Table 3. Spray- and robotic parameters used in experimental phase 3 for deposition of pure copper and steel 316L

Process parameter	Unit	Parameter values		
Coating speed v_c	mm/s	250		500
Nozzle distance a	mm	30		
Spray angle γ	°	0		
Number of tracks n_t	-	10		
Track distance d_t	mm	0.5		1.0
Number of layers n_l	-	2	4	10



Fig. 1. Cold spray system with laser profile sensor

3. MODELLING AND SIMULATION DESIGN

Assadi et al. [1], Raletz et al. [14], and Schmidt et al. [15] examined in detail how particle temperature and velocity affect coating formation in the cold spray process. Because these variables govern particle bonding and coating quality, they are decisive for process performance. Building on this basis, Raletz analyzed the influence of varying process parameters on particle distribution and thereby provided guidance for the optimization of deposition conditions. For cold spray-deposition, the selection of suitable process parameters is essential to obtain a homogeneous deposit. The resulting deposit geometry can generally be approximated by a Gaussian distribution that is strongly affected by both the process parameters and the configuration of the nozzle relative to the substrate. This dependence underlines the need for accurate control of nozzle positioning and operating conditions in order to achieve reproducible results. Klinkov further developed these insights by investigating the interaction of particle distribution, nozzle angle, and the resulting geometry

of additively manufactured components applying a semi-empiric model for the deposition simulation. That study highlighted the importance of nozzle orientation and particle trajectory for defining the deposition profile. According to Klinkov, in equation 1, *De* denotes the deposition efficiency at a discrete position [12]. The parameters k_1 and k_2, characterize the angular dependence of deposition efficiency and the spatial distribution of the particle jet, respectively. The parameter γ_m denotes the limiting spray angle at which the deposition efficiency becomes zero, according to the original formulation. They are dimensionless quantities applied as fitting-parameters, which are adjusted depending on the material under consideration. Therefore, these parameters summarize the variations that occur in real cold-spray processes such as particle size distribution, velocity distribution, temperature differences, oxide layers or surface condition. Their values are material specific and are therefore to be obtained from experimental calibration. These parameters characterize both the particle distribution and the deposition behavior of the spray process. The parameter k_1 describes the dependence of the deposition efficiency on the spray angle γ_n. Hence, this parameter determines the shape of the Gaussian function representing the angular dependence of the deposition efficiency. Consequently, k_1 governs how sensitively the deposition efficiency changes with variations in the spray angle γ_n. The parameter k_2 defines the shape and spread of the Gaussian approximation used to describe the particle distribution. In particular, it determines the width of the distribution and therefore reflects the degree of particle dispersion within the spray plume. In addition, the parameter γ_m represents the critical spray angle at which the deposition efficiency reaches a value of $De = 0$. This angle serves as a characteristic operating point of the spraying process and provides important information regarding the optimal alignment between the spray jet and the target surface. The variable r_n represents the nozzle radius projected onto the substrate, whereas γ_n denotes the angle between the spray line and the contact surface [12]. In the present work, this formulation is used to describe the relative spatial distribution of deposited material. The material-dependent parameters are identified empirically by comparing simulated deposition profiles with experimentally measured profiles. Therefore, the model does not explicitly resolve individual particle impacts or directly determine the deposited mass from powder collection measurements. Instead, the geometric deposition response is calibrated against the experimentally observed material build-up.

$$De = \begin{cases} \dfrac{e^{-k_1(\tan\cdot\gamma_n/\tan\cdot\gamma_m)^2}-e^{-k_1}}{1-e^{-k_1}} \cdot \dfrac{e^{-k_2(r/r_n)^2}-e^{-k_2}}{1-e^{-k_2}} & r < r_n \text{ and } \gamma_n < \gamma_m \\ 0 & \text{else} \end{cases} \tag{1}$$

The numerical surface increment is determined by the deposition model, considering the powder mass flow rate $\dot{m}_p$, deposition efficiency D_e, coating speed v_c, and spatial particle distribution. The deposited material volume is proportional to the powder mass flow rate and deposition efficiency, while the coating speed v_c determines the local exposure time and, consequently, the deposited volume per unit travel distance. The resulting material increment is distributed across the surface according to the Gaussian deposition profile, accounting for the local spray angle γ_n and material-specific parameters. Accordingly, the local surface

height increment increases with increasing powder mass flow rate $\dot{m}_p$ and deposition efficiency *De*, whereas a higher coating speed reduces the deposited material per unit travel distance. The numerical discretization step is distinguished from the physical material increment, which represents the actual surface build-up. During each iteration, the calculated material increment is superimposed onto the existing surface geometry, thereby updating the local surface profile and spray angle γ_n for subsequent deposition steps.

For this work, the basic principles of the model by Klinkov were used and supplemented to develop the deposition simulation illustrated with Fig. 2. Figure 2a indicates that the spray plume forms a conical volume rather than a cylindrical one because of the nozzle divergence angle embedding the particle distribution by the Gaussian approximation in regard to equation 1 [16]. As a result, the coated surface is dependent on the distance *a* between the nozzle and the workpiece. The fitting parameters used for the modelling of the deposition profile specified for the materials steel 316L are $k_{1,St} = 0.0164$ and $k_{2,St} = 21.9$ as well as $k_{1,Cu} = 0.0196$ and $k_{2,Cu} = 19.9$ for pure copper respectively.

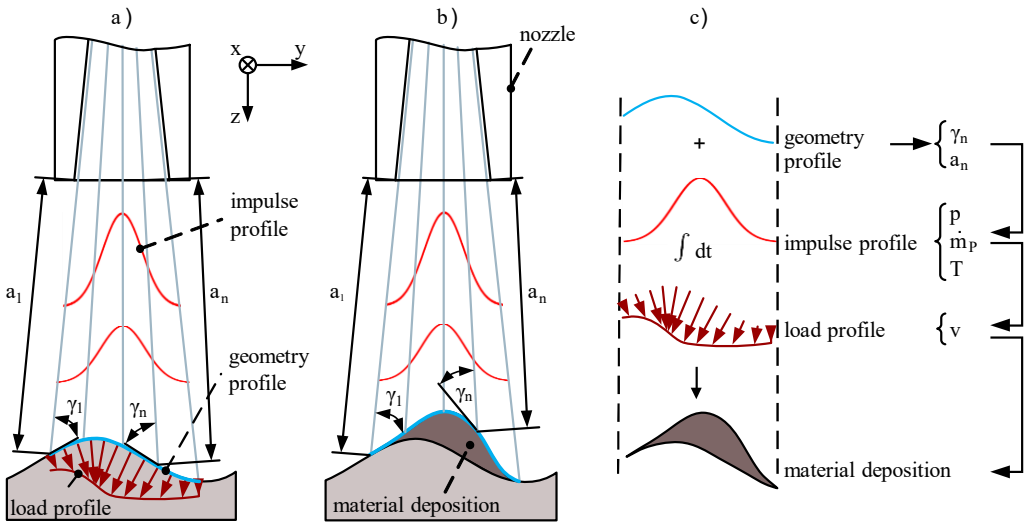


Fig. 2. Theoretical model; a) depiction of impulse profile and load profile; b) updated surface with material increment after deposition; c) summary of simulation approach

As discussed above, another key factor affecting material deposition is the spray angle γ_n, since it governs the deposition efficiency. Figure 2b shows that, during the process, the workpiece surface is continuously updated as each additional layer is deposited, which in turn causes variations in the spray angle γ_n, which is defined as the relative angle between the spray direction vector and the surface normal vector. These surface updates therefore have to be taken into account in the subsequent stage of the simulation.

Figure 2c summarizes the general simulation concept. The material deposition is determined from the spray angle γ_n and the particle distribution. In the illustration, the load profile represents the robotic motion. It is assumed that the particle deposition rate per unit time is known from the material feed rate $\dot{m}_p$. When the robot velocity is reduced, a given area of the workpiece remains exposed to the nozzle for a longer time, which leads to an increased material deposition.

The model described above is used to establish a simulation tool for cold spray deposition (Fig. 3). Building upon the single-layer deposition model introduced above, the simulation of deposition is discretized into successive multilayer. Consequently, the simulation is conducted using a layer by layer discretization approach.

In practical applications, the coating speed v_c and the material feed rate $\dot{m}$ are specified to achieve a target deposition. Consequently, the material increment in the two-dimensional model is expressed as a function of these parameters rather than being directly time-dependent. Therefore, time is not treated as an explicit variable in the simulation. The discretization is thus defined in terms of v_c and $\dot{m}$. If the product of these parameters increases, the discretization step size in the simulation is increased accordingly, assuming a linear relationship. This approach is advantageous for industrial applications, as it establishes a direct link between process parameters and deposition behavior, thereby facilitating efficient parameter identification.

Figure 3 presents the result of a 2D-deposition simulation for copper using a gas temperature of $T_{N2,cu}$ = 750°C and a gas pressure of $p_{N2,cu}$ = 5 MPa. At every discrete simulation step, material is deposited onto the existing geometry. This behavior is governed by factors including the material specific parameters k_1 and k_2, and the spray angle γ_n as shown in equation 1. From the surface normal vector and the spray direction vector, the spray angle γ_n is obtained. The region between the dotted line and the blue line corresponds to the material deposited during a single simulation step. Throughout the simulation, this area increases significantly because of the particle distribution and the high deposition efficiency associated with orthogonal impact.

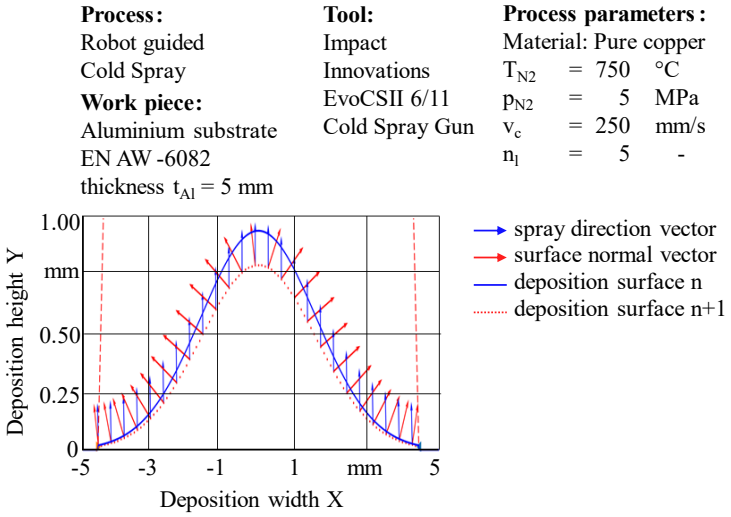


Fig. 3. 2D-simulation of a perpendicular multi-layer cold spray deposition on a planar substrate

Because the surface geometry gradient is a relevant factor in the calculation of a material increment, the surface is represented by a set of points, which are organized as a two-dimensional array in the simulation. As material accumulates, the simulation relocates existing points from the previous simulation step to represent the updated substrate surface. Additional points are generated in regions where the distance between neighboring points is

large in order to improve the surface resolution. This approach maintains a relatively stable number of data points throughout the simulation. Compared to mesh-based methods, this also allows for the insertion of additional points in regions where a higher resolution is required due to material accumulation. As a consequence, the proposed method exhibits improved computational efficiency and reduced memory requirements compared to conventional approaches, such as mesh-based simulations.

4. RESULTS

All experiments were conducted three times in a randomized manner for statistical robustness. For the measurement data acquisition, each specimen was scanned at five consecutive positions with a laser profile sensor as described above. Hence, 15 measurements were taken in order to determine an arithmetic mean deposition 2D-profile for any parameter set. Each scan-profile consists of 3,200 data points over a profile length of L_{LP} = 80 mm, each one reflecting one height-information in the data set, resulting in a virtual representation of the deposition profile of a cold spray specimen. For the purposes of the investigations presented here, the profile geometry was measured following the completion of the specified tracks or layers. No measurements of the profile height were taken between successive layers. Hereafter, results of the first three experimental phases are presented. Each of the acquired mean deposition profiles for the shown parameter sets is compared to a simulated profile from the 2D-simulation model.

As described above, in the first experimental phase, single deposition tracks were used as a baseline evaluation of the particle distribution in straight spray tracks in dependence on the varied process parameters. Figure 4 presents a comparison between the measured mean value and the simulated cross-sectional profiles of single deposition tracks for steel 316L and pure copper at coating speeds of 250 mm/s $\leq v_c \leq$ 500 mm/s. For both materials, the deposited profiles exhibit an approximately Gaussian morphology, with the maximum deposition height located in the central region of the spray track and a gradual decrease toward the track boundaries. The standard deviation for the measured deposition height is 0.005 mm < σ_{St} < 0.007 mm for steel 316L and 0.006 mm < σ_{Cu} < 0.009 mm for copper for the three coating velocities v_c. Increasing the coating speed leads to a systematic reduction in deposition height, which can be attributed to the shorter local exposure time of the substrate to the particle jet. In absolute terms, copper exhibits higher deposition heights than steel 316L across the investigated parameter range. This behavior is partly associated with the higher material feed rate used for copper, $\dot{m}_{Cu}$ = 5.9 kg/h, compared with $\dot{m}_{St}$ = 5.0 kg/h. Nevertheless, the height difference is not proportional to the feed-rate ratio, indicating additional material-specific influences such as deposition efficiency, particle deformation behavior, and profile broadening. In the simulation, these effects are considered in the factors k_1 and k_2 as described above. The value of the mean relative profile-error of the simulation with respect to the measurement equals $E_{St,vc}$ = 10.78 % for steel 316L and $E_{Cu,vc}$ = 16.55 % for copper. The relative profile-error values are averaged over the three coating velocities v_c. Overall, the simulation captures the velocity-dependent trends and profile shapes with acceptable agreement. In both cases, the resulting relative simulation error

is caused by the low total deposition height in the single-track experiments, which causes a high relative standard deviation in the measured values.

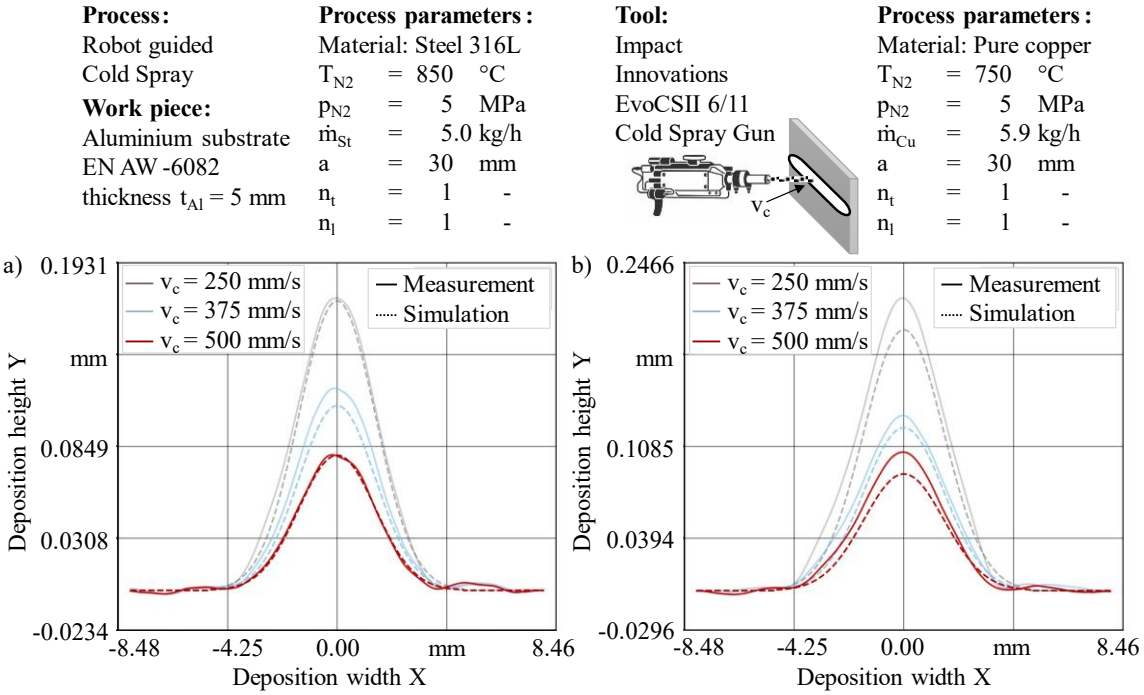


Fig. 4. Comparison of simulation and measurement data from perpendicular single track cold spray deposition experiments; a) deposition material steel 316L; b) deposition material pure copper

Figure 5 compares measured and simulated cross-sectional profiles for multi-track cold spray deposition of steel 316L and pure copper at different track distances d_t. For both materials, the deposition height increases markedly with decreasing track distance, which can be attributed to the stronger overlap of adjacent spray tracks. The standard deviation for the measured deposition height is $0.022\ \text{mm} < \sigma_{St} < 0.037\ \text{mm}$ for steel 316L and $0.019\ \text{mm} < \sigma_{Cu} < 0.034\ \text{mm}$ for copper for the three track distances d_t. At $d_t = 0.5$ mm, the profiles exhibit a pronounced central peak, whereas larger track distances lead to broader and flatter deposition geometries. In absolute terms, steel 316L shows higher maximum deposition heights than copper, particularly for small track distances. This behavior is consistent with the material feed rates used in the multi-track experiments, where $\dot{m}_{St} = 5.0$ kg/h exceeds $\dot{m}_{Cu} = 4.2$ kg/h. However, the observed differences cannot be explained solely by the feed-rate ratio, since deposition efficiency, particle-substrate interaction, and lateral material distribution also influence the resulting profile. The value of the mean relative profile-error of the simulation with respect to the measurement equals $E_{St,dt} = 4.43$ % for 316L-steel and $E_{Cu,dt} = 5.83$ % for copper. The relative profile-error values are averaged over the three track distances d_t. Overall, the simulation reproduces the measured profile shapes and the track-distance-dependent trends with good agreement, with minor deviations mainly occurring in the flank regions and at the transition between adjacent tracks.

Figure 6 compares measured and simulated cross-sectional profiles for multi-layer cold spray deposition for different numbers of deposited layers n_l and track distances d_t. For both materials, the deposition height increases systematically with increasing layer number, confirming the cumulative character of the layer-wise material build-up.

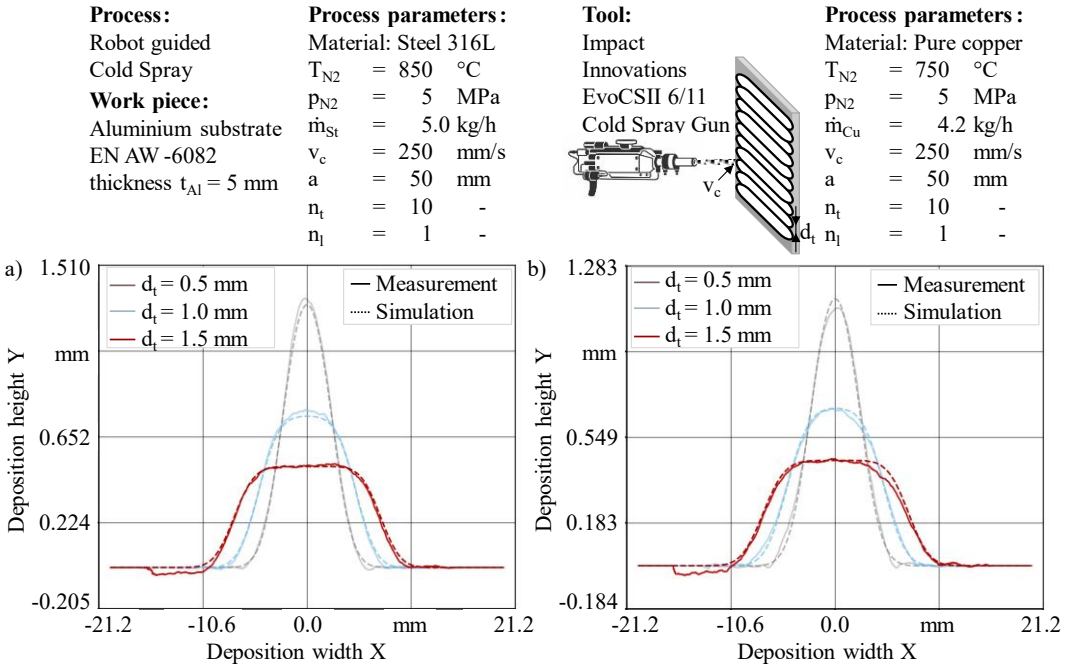


Fig. 5. Comparison of simulation and measurement data from perpendicular multi-track cold spray deposition experiments; a) deposition material steel 316L; b) deposition material pure copper

The increase is particularly pronounced for $n_l = 10$, where the profiles exhibit a substantially higher central deposition region compared with $n_l = 2$ and $n_l = 4$. The standard deviation for the measured deposition height is 0.042 mm < σ_{St} < 0.061 mm for steel 316L and 0.073 mm < σ_{Cu} < 0.101 mm for copper for the three numbers of layers n_l and for the track distance $d_t = 0.5$ mm. For the three numbers of layers n_l and for track distance $d_t = 1.0$ mm the standard deviation for the measured deposition height is 0.028 mm < σ_{St} < 0.116 mm for steel 316L and 0.044 mm < σ_{Cu} < 0.126 mm for copper. In addition, the track distance d_t influences the resulting geometry. Smaller track distances lead to stronger overlap between adjacent tracks and therefore to higher and more concentrated deposition profiles, whereas larger track distances result in a slightly broader and lower material build-up.

In absolute terms, steel 316L reaches greater deposition heights than copper for comparable layer numbers and track distances. This can partly be attributed to the higher material feed rate used for steel in the multi-layer experiments, with $\dot{m}_{St} = 5.0$ kg/h, compared with $\dot{m}_{Cu} = 4.2$ kg/h. However, the differences in profile height and shape also indicate material-specific effects, including deposition efficiency, particle deformation behavior, and the evolution of the local surface geometry during repeated over-spraying.

The value of the mean relative profile-error of the simulation with respect to the measurement equals $E_{St,dt=0.5\ mm} = 16.15$ % for the track distance $d_t = 0.5$ mm and $E_{St,dt\ =\ 1.0\ mm} = 6.20$ % for the track distance $d_t = 1.0$ mm for steel 316L. For copper the value of the mean relative profile-error of the simulation with respect to the measurement is

$E_{Cu,dt=0.5\ mm}$ = 16.34 % for the track distance d_t = 0.5 mm and $E_{Cu,dt=1.0\ mm}$ = 14.22 % for the track distance d_t = 1.0 mm. The relative profile-error values are averaged over the three numbers of layers n_l. The simulation reproduces the general layer-dependent trends and the overall profile morphology with acceptable agreement. The main part of the mean relative profile error is caused by deviations in the peak region, particularly for layer number n_l = 10, where inaccuracies in each deposited layer accumulate. This indicates that the model is suitable for predicting multi-layer deposition behaviour, while further refinement is required to improve accuracy for high build-up geometries.

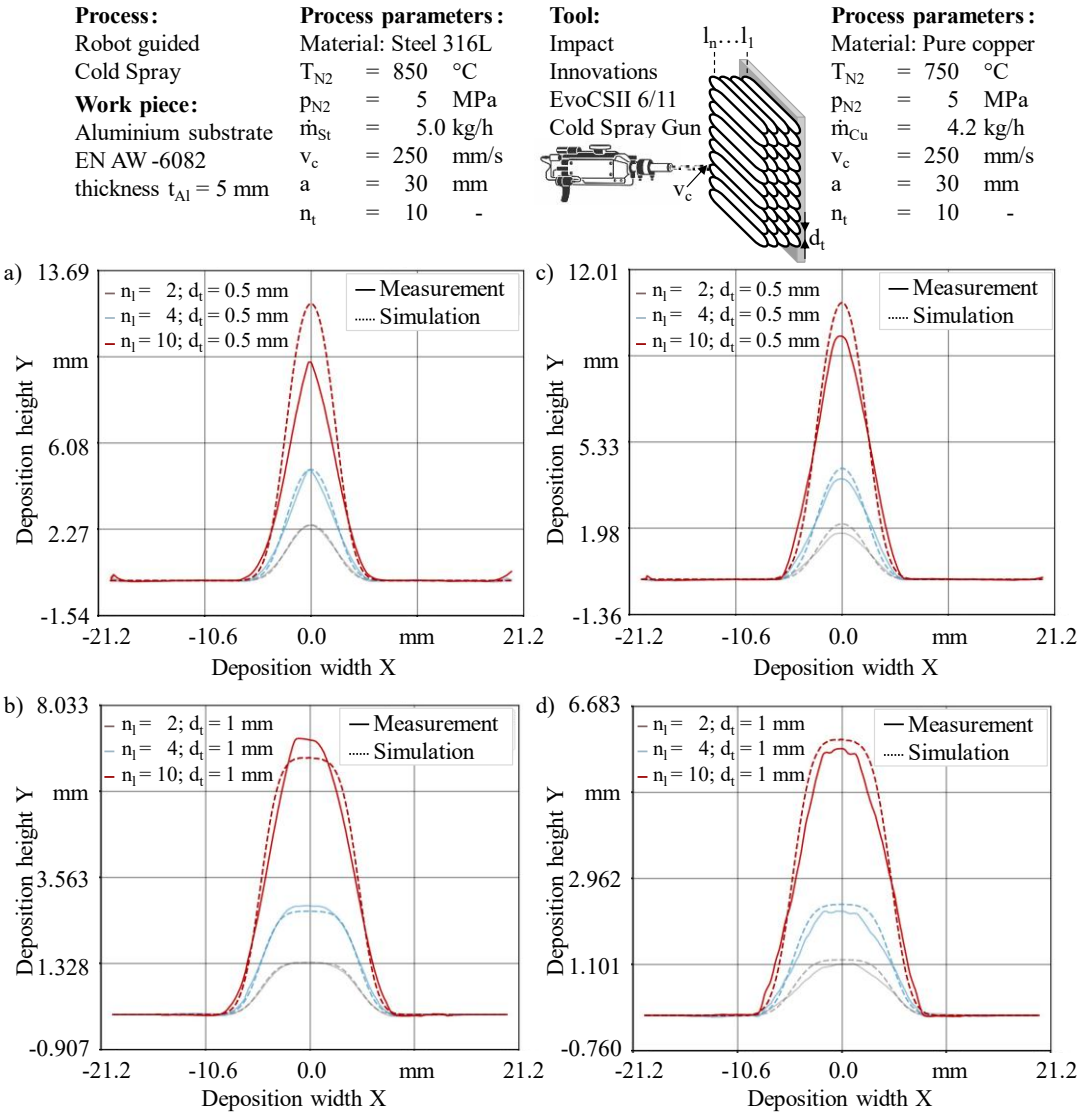


Fig. 6. Comparison of simulation and measurement data from perpendicular multi-layer cold spray deposition experiments; a) deposition material steel 316L with a track distance d_t = 0.5 mm; b) deposition material steel 316L with a track distance d_t = 1.0 mm; c) deposition material copper with a track distance d_t = 0.5 mm; d) deposition material copper with a track distance d_t = 1.0 mm

5. SUMMARY

This study presents a simulation-based approach for predicting material deposition in cold spray additive manufacturing. A 2D-deposition model was developed and validated experimentally for stainless steel 316L and pure copper on planar aluminium substrates. The model considers relevant process parameters, including coating speed, material feed rate, track distance, number of tracks, and number of deposited layers. Experimental validation was performed using laser profile measurements, allowing direct comparison between measured and simulated cross-sectional deposition profiles. The results show that the simulation captures the characteristic Gaussian-like profile morphology of single tracks as well as the cumulative build-up behavior in multi-track and multi-layer deposition. For both materials, the model reproduces the main trends associated with coating speed, track overlap, and layer number with acceptable agreement. Deviations occur in regions with high local deposition, where layer-wise inaccuracies accumulate. To address this, further research on non-planar substrates still has to be carried out. Once the prediction capability of the introduced 2D-simulation tool has been further improved, a 3D-simulation tool can be established and validated. Overall, the presented approach provides a suitable basis for simulation-supported tool path planning to be applied for adaptive process control in robot-guided cold spray additive manufacturing.

ACKNOWLEDGEMENT

This research work was funded by the Investitionsbank Berlin (IBB) with co-financing by the European Regional Development Fund (ERDF).

Kofinanziert von der Europäischen Union

REFERENCES

[1] ASSADI H., KREYE H., GÄRTNER F., KLASSEN T., 2016, *Cold Spraying - a Materials Perspective*, Acta Materialia, 116, 382–407.

[2] BRAUN T., UHLMANN E., HÄCKER R., JÄGER M., RAUCH H., BRACH K., et al., 2022, *Evaluation of Electric Conductivity and Mechanical Load Capacity of Copper Deposits for Application in Large Winding Components for Electrical High-Voltage Machines Made with Cold Spray Additive Manufacturing*, Thermal Spray 2022: Proceedings from the International Thermal Spray Conference, Vienna, Austria, 743–749.

[3] KAFLE A., SILWAL R., KOIRALA B., ZHU W., 2024, *Advancements in Cold Spray Additive Manufacturing: Process*, Materials, Optimization, Applications, and Challenges, Materials, 17/22, 5431.

[4] JAQUEMOD A., PALALIĆ M., GÜZEL K., MÖHRING H.-C., 2024, *In-Process Monitoring of Inhomogeneous Material Characteristics Based on Machine Learning for Future Application in Additive Manufacturing*, Journal of Machine Engineering, 24/2, 83–93.

[5] SUN W., CHU X., LAN H., HUANG R., HUANG J., XIE Y., et al., 2022, *Current Implementation Status of Cold Spray Technology: A Short Review*, Journal of Thermal Spray Technology, 31/4, 848–865.

[6] ASHOKKUMAR M., THIRUMALAIKUMARASAMY D., SONAR T., DEEPAK S., VIGNESH P., ANBARASU M., 2022, *An Overview of Cold Spray Coating in Additive Manufacturing, Component Repairing and Other Engineering Applications*, Journal of the Mechanical Behavior of Materials, 31/1, 514–534.

[7] EL-QEMARY A., KABBOURI I., BOUTAHARI S., CHAHBOUNI M., 2025, Anticipation and Correction of Additive Manufacturing Geometric Defects at the Design Stage, Journal of Machine Engineering, 25/2, 74–88.

[8] BRAUN T., BEHREND O., SCHWANDT A., BARNICK N., ELLIESEN U., PAVEL D., UHLMANN E., 2024, *Additiv Gefertigter Leichtbau für Schienenfahrzeuge: Topologieoptimierte Leichtbaustrukturen zur Versteifung von Fahrzeugsegmenten im Schienenverkehr*, Zeitschrift für wirtschaftlichen Fabrikbetrieb, 119/7–8, 534–538.
[9] BALIDAS A., KERBRAT O., HASCOET J.-Y., 2024, *The Potential of Additive Manufacturing of Metal Components to Reduce Environmental Impacts*, Journal of Machine Engineering, 24/2, 94–104.
[10] REMY A., NWANKPA U.-V., RAUCH M., HASCOËT J.-Y., RUCKERT G., 2024, *Impact of a Variation in Wire Feed Speed on Deposits From the Wire Arc Additive Manufacturing (WAAM)*, Journal of Machine Engineering, 24/2, 117–128.
[11] UHLMANN E., POLTE M., BLUMBERG J., SOBIAK O., 2026, *Real-Time Direct Pose Control of Industrial Robots with Proprietary Robot Controller Based on a Redundant Camera Tracking System*, Procedia CIRP, 138, 280–285.
[12] KLINKOV S.V., KOSAREV V.F., SHIKALOV V.S., 2019, *Control of Cold Spray Process by Changing of Nozzle Setting Angle*, Proceedings of the XXVI Conference on High-Energy Processes in Condensed Matter, Novosibirsk, Russia, 020022–1–020022–5.
[13] CHEN C., XIE Y., VERDY C., LIAO H., DENG S., 2017, *Modelling of Coating Thickness Distribution and its Application in Offline Programming Software*, Surface and Coatings Technology, 318, 315–325.
[14] RALETZ F., VARDELLE M., EZO'O G., 2006, *Critical Particle Velocity Under Cold Spray Conditions*, Surface and Coatings Technology, 201/5, 1942–1947.
[15] SCHMIDT T., GAERTNER F., KREYE H., 2006, *New Developments in Cold Spray Based on Higher Gas and Particle Temperatures*, Journal of Thermal Spray Technology, 15/4, 488–494.
[16] UHLMANN E., BRAUN T., ZHANG X., 2025, *Deposition Simulation for an Automated Cold Spray Additive Manufacturing Process*, Thermal Spray 2025: Proceedings from the International Thermal Spray Conference, Vancouver, Canada, 112–119.